Journal of Power Sources 246 (2014) 84–89

Contents lists available at ScienceDirect

Journal of Power Sources

journal homepage: www.elsevier.com/locate/jpowsour

Short communication

# Modeling dendrite growth during lithium electrodeposition at sub-ambient temperature

Rohan Akolkar*

*Department of Chemical Engineering, Case Western Reserve University, A.W. Smith Building, Room 127, 10900 Euclid Avenue, Cleveland, OH 44106, United States*

## HIGHLIGHTS

- Electrochemical model of enhanced Li dendrite growth at sub-ambient temperature.
- Model combines temperature effects on $Li^+$ diffusion and surface film formation.
- Model predicts critical temperature below which dendrite formation is initiated.
- Critical temperature defines the lowest temperature for safe Li-battery operation.

## ARTICLE INFO

*Article history:*
Received 28 April 2013
Received in revised form
12 July 2013
Accepted 14 July 2013
Available online 23 July 2013

*Keywords:*
Lithium electrodeposition
Dendrites
Diffusion
Solid electrolyte interface
Temperature effects

## ABSTRACT

Increased propensity for dendritic lithium electrodeposition during sub-ambient temperature operation has been widely reported in lithium battery systems, yet is not fully understood. In the present paper, a mathematical model is developed to quantify the dendritic growth rate during lithium electrodeposition at sub-ambient temperature. This model builds on a diffusion–reaction framework presented recently by Akolkar [J. Power Sources 232 (2013) 23–28]. Using a steady-state diffusion model with a concentration-dependent diffusion coefficient, the lithium-ion concentration depletion in the stagnant Nernst diffusion boundary layer near the lithium surface is modeled. A surface electrochemical reaction model is then employed to correlate the lithium concentration depletion to the dendrite growth rate. Temperature effects on the lithium-ion transport and its electrochemical surface reaction are incorporated in the model via an Arrhenius-type temperature-dependence of the diffusion coefficient and the apparent charge transfer coefficient. It is shown that lowering the system temperature has the effect of increasing the lithium-ion diffusion resistance and decreasing the surface film thickness – conditions favorable for the formation of dendrites during lithium electrodeposition.



## 1. Introduction

Lithium (Li) electrodeposition is of great importance to current and future generation battery technology. Emerging high energy density Li–$O_2$ (lithium–oxygen) and Li–S (lithium–sulfur) batteries consist of anodes that undergo lithium electrodeposition during charging [1,2]. However, surface morphology evolution in the form of needle-like dendrites can compromise battery safety and degrade cycleability. In the context of conventional lithium-ion (Li-ion) batteries too, dendrite formation is a major concern [3–5]. In fact, it is believed to be one of the potential root causes for the recent lithium-ion battery failures on the Boeing 787 Dreamliner [5]. Thus, there is growing interest in understanding the physicochemical processes that lead to the formation of lithium dendrites during battery charging.

The morphology evolution during lithium electrodeposition depends on a number of system parameters, such as the deposition current density, electrolyte composition, and the presence of additives [6–10]. In addition to these parameters, the role of temperature on the dendritic growth process has also been the subject of numerous experimental investigations, notably by Ota et al. [11,12]. These investigators observed dendritic morphology and concurrent deterioration of anode cycleability at sub-ambient temperatures (typically 0 °C). Additionally, Mogi et al. [13] showed via *in situ* atomic force microscopy that the solid electrolyte interface (SEI) layer on the lithium surface is sensitive to temperature. At elevated temperatures (60–80 °C), the SEI layer transforms into a uniform compact layer that suppresses the

* Tel.: +1 216 368 4151.
*E-mail address:* rna3@case.edu.

0378-7753/$ – see front matter © 2013 Elsevier B.V. All rights reserved.
http://dx.doi.org/10.1016/j.jpowsour.2013.07.056

dendritic growth morphology and enables smooth electrodeposits. These observations clearly highlight the need for improved understanding and characterization of the temperature-dependent physicochemical effects causing lithium dendritic growth at sub-ambient temperature conditions under which lithium batteries are often deployed.

In conjunction with the aforementioned experimental studies, modeling investigations of the dendritic growth during lithium electrodeposition have also been reported [14–16]. Brissot et al. [14] and Chazalviel [15] have employed theoretical modeling to characterize the phenomena underlying the experimentally observed 'onset time for dendrite initiation'. The most notable work on modeling was presented by Monroe and Newman [16], who developed a comprehensive theory of the lithium dendritic growth process in lithium-polymer cells. Akolkar [17] recently extended this model to liquid electrolytes by incorporating the concentration-dependence of the diffusion coefficient [18]. The model by Akolkar [17] provided approximate analytical expressions of the dendrite growth rate, *i.e.*, the dendrite tip current density, as a function of the various system parameters: the applied current density, the bulk lithium concentration, the diffusion coefficient and the cathodic charge transfer coefficient.

In the present work, the analytical model by Akolkar [17] is developed further to incorporate temperature effects. Temperature affects transport in the electrolyte (through its effect on viscosity and ion association) as well as surface electrochemical kinetics (through its effect on the SEI thickness). These dependencies are incorporated in the present model. The model yields an analytical expression for the dendrite growth rate ratio, which is used as a parameter to quantify the propensity for dendritic growth. This parameter is both temperature-dependent and plating rate-dependent, and thus can be used to assess the 'safety window' in terms of temperature and plating current density to suppress dendrites.

## 2. Dendrite growth model

The present model is an extension of the diffusion–reaction model proposed by Akolkar [17]. The detailed model development and justification of underlying assumptions can be found in Ref. [17]. However, to present a self-contained analysis herein, a brief outline of the model by Akolkar is presented below.

Consider, for example, a flat electrode surface on which lithium is being electrodeposited (Fig. 1). A stagnant Nernst diffusion boundary layer (of thickness $\delta$) exists in the proximity of the electrode, transport of lithium ions through which is governed by diffusion. Assuming one-dimensional transport, Fick's second law of diffusion takes the form:

$$\frac{\partial C}{\partial t} = \frac{\partial}{\partial z}\left(D\frac{\partial C}{\partial z}\right) \tag{1}$$

In Eq. (1), $C$ is the lithium-ion concentration in the electrolyte, $D$ is the diffusion coefficient, $z$ is the space dimension and $t$ is the time. Stewart and Newman [18] have shown that the diffusion coefficient is an exponential function of concentration: $D = ae^{-bC}$ (where $a = 2.582 \times 10^{-5}$ cm$^2$ s$^{-1}$ and $b = 2.856$ M$^{-1}$ at room temperature). Moreover, the transient diffusion process, as shown by Akolkar [17], occurs over a relatively short time duration of $\tau = \delta^2/a$. Taking $\delta$ as 400 μm, $\tau$ is estimated to be only about 62 s. Beyond this time-scale, concentration variation with time is negligible, yielding a steady-state diffusion equation:

$$a\frac{\partial}{\partial z}\left(e^{-bC}\frac{\partial C}{\partial z}\right) = 0 \tag{2}$$

At steady state, the concentration at the outer edge of the boundary layer ($z = \delta$ as shown in Fig. 1) is equal to the bulk concentration ($C_0$). At the electrode surface ($z = 0$), the concentration gradient is proportional to the deposition flux. These arguments lead to the following boundary conditions:

$$\text{At } z = \delta: \quad C = C_0 \tag{3}$$

$$\text{At } z = 0: \quad D\frac{\mathrm{d}C}{\mathrm{d}z} = \frac{i_f(1-t_+)}{nF} \tag{4}$$

In Eq. (4), $i_f$ represents the deposition current density on the flat electrode surface (see Fig. 1) and $t_+$ represents the $Li^+$ transport number. Using the above boundary conditions, Eq. (2) can be solved analytically. This provides the concentration depletion ratio, *i.e.*, the ratio of the concentration at the electrode surface to the bulk concentration:

$$\frac{C_e}{C_0} = -\frac{1}{bC_0}\ln\left[e^{-bC_0} + \frac{i_f(1-t_+)b\delta}{nFa}\right] \tag{5}$$

By definition, the limiting current density is approached when $C_e = 0$. Thus, from Eq. (5), the limiting current density on the flat surface is:

$$i_{L,f} = \frac{nFa\left(1-e^{-bC_0}\right)}{(1-t_+)b\delta} \tag{6}$$

Let us now assume that a lithium 'dendrite precursor' or 'roughness element' exists on the flat lithium surface (as shown in Fig. 1) from which a dendrite propagates. It is assumed that the dendrite precursor occupies only a small fraction of the electrode surface area; thus, it does not significantly alter the concentration profile within the diffusion boundary layer [17]. Furthermore, since the net current consumed by the dendrite tip is small, the flat electrode current density ($i_f$) continues to be a reasonable estimate of the average lithium plating current density [17]. On the flat lithium surface, the net overpotential ($\eta_f$) is due to activation and concentration polarization [19]:

$$\eta_f = \eta_{a,f} + \eta_{c,f} = \frac{RT}{\alpha_c F}\ln\left(\frac{i_f}{i_0}\right) - \frac{RT}{nF}\ln\left(\frac{C_e}{C_0}\right) \tag{7}$$

The negative sign preceding the concentration overpotential term is inserted to conserve its positive value, consistent with the sign convention employed. In Eq. (7),$i_0$ is the exchange current density and $\alpha_c$ is the cathodic charge transfer coefficient. It has been

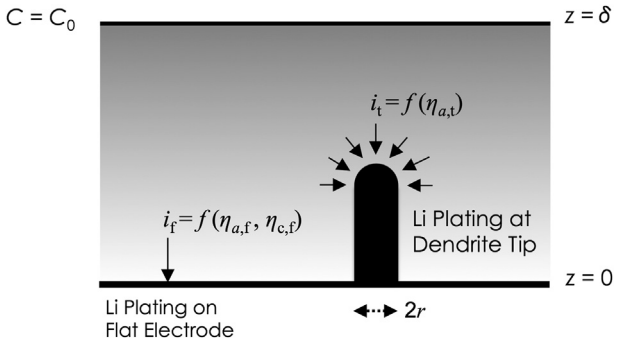


**Fig. 1.** Schematic of the electrode surface on which lithium is electrodeposited. A small micron-scale dendrite precursor is also shown (not to scale). While electrodeposition on the flat surface (at rate $i_f$) is driven by the activation ($\eta_{a,f}$) and concentration ($\eta_{a,f}$) overpotentials, the electrodeposition at the dendrite tip (at rate $i_t$) is purely under activation control ($\eta_{a,t}$) due to 'spherical diffusion' to the small dendrite tip.

shown, in several electrodeposition systems [17,20,21], that the dendrite tip grows purely under activation control. This is due to 'spherical diffusion' to the dendrite tip, which eliminates concentration polarization at the tip. Additionally, as shown by Akolkar [17] for micron-scale dendrites, the surface overpotential due to the radius of curvature of a dendrite tip is negligible in the lithium system. This leads to the following approximation for the dendrite tip overpotential:

$$\eta_t \cong \eta_{a,t} = \frac{RT}{\alpha_c F}\ln\left(\frac{i_t}{i_0}\right) \tag{8}$$

In Eq. (8), $i_t$ is the dendrite tip current density. The overpotential at the flat electrode surface and the dendrite tip overpotential are essentially identical [17]. This is due to the fact that the substrate is highly conductive and the ohmic potential difference (in solution) between the tip and the flat surface is negligible. Thus, one may equate the net overpotentials given by Eqs. (7) and (8), providing:

$$\frac{i_t}{i_f} = \left(\frac{C_e}{C_0}\right)^{-\alpha_c/n} \tag{9}$$

Inserting the expression for $C_e/C_0$ and $i_{L,f}$ from Eqs. (5) and (6) into Eq. (9) gives:

$$\frac{i_t}{i_f} = \left\{-\frac{1}{bC_0}\ln\left[e^{-bC_0} + \frac{i_f}{i_{L,f}}\left(1 - e^{-bC_0}\right)\right]\right\}^{-\alpha_c/n} \tag{10}$$

Eq. (10) is the central equation in the present model. It provides an analytical expression for the dendrite growth rate ratio ($i_t/i_f$) and can be used to assess the propensity for dendritic growth in the system. The ratio depends on several system parameters: (i) the bulk concentration ($C_0$); (ii) the fraction of the Li plating current density ($i_f$) with respect to the system limiting current density ($i_{L,f}$); and (iii) the cathodic charge transfer coefficient ($\alpha_c$) representing the kinetics of lithium electrodeposition.

## 3. Effect of temperature on the dendrite growth rate ratio

The objective of the present manuscript is to characterize the effect of temperature on the dendrite growth rate, *i.e.*, the ratio $i_t/i_f$, during lithium electrodeposition. At sub-ambient temperature conditions, the ratio $i_t/i_f$ increases due to two primary factors:

(i) *Transport* – At sub-ambient temperature, the viscosity of the non-aqueous electrolyte increases with decreasing temperature. Increase in viscosity lowers the effective diffusion coefficient [22,23]. Furthermore, at sub-ambient temperature, increased ion association may further impede transport via diffusion [18]. The net increase in the diffusion resistance manifests as a lower limiting current density ($i_{L,f}$) in Eq. (10) and thus a larger dendrite growth rate ratio ($i_t/i_f$).

(ii) *Reaction* – At lower temperatures, the solid electrolyte interface (SEI) layer formed on the electrode surface is thinner. As shown below, the lower SEI thickness provides an effectively larger cathodic transfer coefficient ($\alpha_c$). Increase in $\alpha_c$ results in an increase in the dendrite growth rate ratio $i_t/i_f$ [17] according to Eq. (10).

To model the two aforementioned effects of temperature on the dendrite growth rate, let us define quantitatively the temperature-dependence of the diffusion coefficient and the charge transfer coefficient. To define the temperature-dependence of the diffusion coefficient, let us assume that the diffusion pre-exponent '$a$' is temperature-dependent. Since the diffusion coefficient is typically inversely proportional to viscosity [18], and since viscosity follows an Arrhenius-type temperature-dependence [24] in many non-aqueous electrolytes, one can express the diffusion pre-exponent '$a$' as:

$$a = a_0\exp\left[\frac{E_D}{R}\left(\frac{1}{T_0} - \frac{1}{T}\right)\right] \tag{11}$$

This temperature-dependence of the diffusion coefficient is consistent with the experimental findings of Nishida et al. [25] for several lithium-salts in organic electrolytes. In Eq. (11), $a_0$ is a temperature-independent pre-exponent, $E_D$ is the activation energy, $R$ is the universal gas constant, $T_0$ is a reference temperature at which $a = a_0$, and $T$ is the system temperature. In the present work, $T_0$ was selected to be the room temperature (298 K) at which the pre-exponent $a_0$ becomes $2.582 \times 10^{-5}$ cm$^2$ s$^{-1}$, according to Stewart and Newman [18]. The activation energy $E_D$ was set to 33 KJ mol$^{-1}$, estimated based on the temperature-dependence of diffusion coefficient observed by Valoen and Reimers [22] for a multi-component solvent mixture. This value is somewhat higher than that reported by Nishida et al. (~20 KJ mol$^{-1}$) for a single component solvent [25]. Combining Eq. (11) with the concentration-dependence of the diffusion coefficient ($D = ae^{-bC}$) provides:

$$D = a_0\exp\left[-bC + \frac{E_D}{R}\left(\frac{1}{T_0} - \frac{1}{T}\right)\right] \tag{12}$$

The temperature- and concentration-dependence of the diffusion coefficient is shown in Fig. 2. It is observed that the diffusion coefficient decreases with increasing concentration, much in accordance with the experimental values reported by Stewart and Newman [18]. At a given concentration, the diffusion coefficient depends exponentially on $T^{-1}$ in agreement with observations of Valoen and Reimers [22].

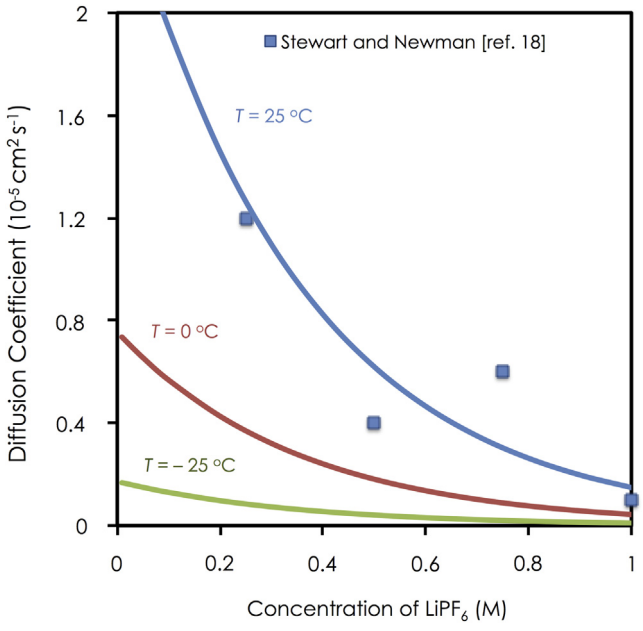


**Fig. 2.** Diffusion coefficients, calculated using Eq. (12), as a function of the $LiPF_6$ concentration and the electrolyte temperature (solid lines). The diffusion coefficient decreases at sub-ambient temperature. Blue square dots represent experimentally measured diffusion coefficient data from Stewart and Newman [18] (For interpretation of the references to colour in this figure legend, the reader is referred to the web version of this article).

Let us now characterize the temperature-dependence of the cathodic charge transfer coefficient. According to the Tafel equation [19], the current density $i$ is related to the overpotential $\eta_a$ by:

$$i = i_0 \exp\left(\frac{\alpha_c F}{RT}\eta_a\right) \tag{13}$$

A high cathodic charge transfer coefficient, $\alpha_c$, represents a favorable cathodic (deposition) process over an unfavorable reverse (dissolution) process. During electrodeposition of alkali and alkali earth metals from non-aqueous electrolytes, a surface film (called the 'solid electrolyte interface' or SEI layer) forms at the electrode–electrolyte interface. In the presence of ionic migration through the SEI layer, Peled [26] showed that the Tafel expression takes the form:

$$i = i_0 \exp\left(\frac{\omega n F}{RTl}\eta_a\right) \tag{14}$$

In Eq. (14), $\omega$ incorporates the half-jump distance in the high field ionic migration model of Mott and Cabrera [27], and $l$ is the solid electrolyte interface (SEI) layer thickness. The ratio $\eta_a/l$ is the electric field that develops across the SEI layer. Comparing Eq. (14) to the traditional form of the Tafel expression [Eq. (13)], one gets the following proportionality for the apparent cathodic charge transfer coefficient:

$$\alpha_c \propto \frac{1}{l} \tag{15}$$

Thus, the apparent cathodic charge transfer coefficient, which is a symmetry parameter in classical electrochemical systems, is inversely proportional to the SEI thickness formed on a Li surface during electrodeposition from an organic electrolyte. During SEI film formation, species (*e.g.*, the solvent) diffusion through the SEI layer is regarded as the rate-determining step [26]. Under diffusion-limited SEI growth, the SEI thickness follows a parabolic rate law [26,27]:

$$l = \sqrt{\mathrm{k}D_s t} \tag{16}$$

In Eq. (16), k is a constant, $D_s$ is the solid phase diffusion coefficient of the diffusing species and $t$ is the time. Although the SEI thickness theoretically depends on $t^{0.5}$, in practical systems a relatively constant SEI thickness is reached at large time-scales [28]. Since the dendrite growth occurs on a time-scale that is atleast an order of magnitude larger than the SEI formation time and the unsteady-state $Li^+$ diffusion time constant ($\sim$100 s), a pseudo steady-state condition may be assumed during dendrite propagation. According to Eq. (16), the SEI thickness depends on the diffusion coefficient $D_s$, which in turn exhibits temperature-dependence according to the Eyring model [29]:

$$l \propto \sqrt{D_s} = \sqrt{D_0 \exp\left(-\frac{E}{RT}\right)} \tag{17}$$

In Eq. (17), $D_0$ is a temperature-independent pre-exponent, $E$ is the activation energy and $T$ is the temperature. Combining Eqs. (15) and (17), one gets:

$$\alpha_c \propto \exp\left(-\frac{E}{2RT}\right) \tag{18}$$

Choosing $T_0 = 298$ K as the reference temperature at which the cathodic charge transfer coefficient $\alpha_c^0$ is known [30], one can write the following expression for the temperature-dependent cathodic charge transfer coefficient:

$$\frac{\alpha_c}{\alpha_c^0} = \exp\left[-\frac{E}{2R}\left(\frac{1}{T_0}-\frac{1}{T}\right)\right] \tag{19}$$

The temperature-dependence of the cathodic transfer coefficient is shown in Fig. 3, which indicates that the transfer coefficient increases in magnitude with decreasing temperature. Physically, this indicates a thinning of the 'local' surface SEI layer leading to lower surface polarization locally. Globally, other effects such as macro-scale uniformity and structure of the SEI layer, which are temperature-dependent [13], may produce apparently conflicting trends in measured overall surface resistance. For example, electrochemical impedance measurements by Ota et al. [11,12] show that the surface resistance is in fact increased at lower temperature.

Inserting expressions for the limiting current density from Eq. (6), the diffusion coefficient from Eq. (11) and the cathodic transfer coefficient from Eq. (19), into Eq. (10), we get:

$$\frac{i_t}{i_f} = \left\{ -\frac{1}{bC_0}\ln\left[e^{-bC_0} + \frac{i_f(1-t_+)b\delta}{nFa_0\exp\left\{\Delta_1\left(\frac{1}{T_0}-\frac{1}{T}\right)\right\}}\right]\right\}^{-\left(\alpha_c^0/n\right)\exp\{\Delta_2(1/T_0-1/T)\}} \tag{20}$$

In Eq. (20), $\Delta_1 = E_D/R$ and $\Delta_2 = -E/2R$. Eq. (20) presents a concise analytical form of the temperature-dependent dendrite growth rate ratio $i_t/i_f$. If the transport properties ($a_0$, $b$, $\delta$, $t_+$) and the activation energies for solution phase and solid phase diffusivities

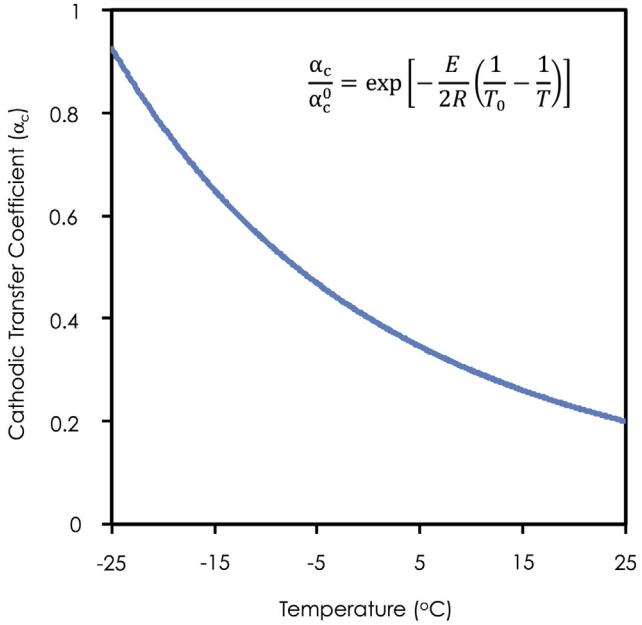


**Fig. 3.** Temperature-dependence of the apparent cathodic charge transfer coefficient, calculated using Eq. (19). The increase in the charge transfer coefficient at sub-ambient temperature is due to a decrease in the SEI thickness.

**Table 1**
Parameter values used in the mathematical model.

| Parameter | Value | Source |
|---|---|---|
| Reference temperature | $T_0 = 298$ K | Selected |
| Diffusion pre-exponent | $a_0 = 2.582 \times 10^{-5}$ cm$^2$ s$^{-1}$ | Ref. [18] |
| Solution phase diffusion activation energy | $E_D = 33$ KJ mol$^{-1}$ | Ref. [22] |
| Transfer coefficient at $T = T_0$ | $\alpha_c = 0.2$ | Ref. [30] |
| SEI-phase diffusion activation energy | $E = 37$ KJ mol$^{-1}$ | Ref. [29] |
| $Li^+$ bulk concentration | $C_0 = 1$ M | Selected |
| Boundary layer thickness | $\delta = 400$ μm | Ref. [31] |
| Transference number | $t_+ = 0.4$ | Ref. [22] |

($E_D$ and $E$) are known, the ratio $i_t/i_f$ can be computed as a function of the applied Li plating rate $i_f$ and the temperature $T$.

## 4. Results and discussion

Parameter values used in the present model are documented in Table 1. Parameter values represent lithium electrodeposition from a widely used non-aqueous electrolyte containing $LiPF_6$ salt in an EC:DMC (1:1 by weight) solvent. In a few instances, such as the activation energies, for which data in the EC:DMC system is not readily available, estimates based on other similar systems were used. Eq. (20) was used to calculate the dendrite growth rate ratio $i_t/i_f$ as a function of the temperature for three different plating current densities as shown in Fig. 4. The three current densities selected were 5 mA cm$^{-2}$, 10 mA cm$^{-2}$ and 15 mA cm$^{-2}$. It is seen that the ratio $i_t/i_f$ is small ($i_t/i_f \rightarrow 1$) at all operating current densities when the temperature is near ambient ($\sim$25 °C). However, as the temperature decreases, the ratio $i_t/i_f$ increases gradually until a critical temperature is reached. Near the critical temperature, the dendrite growth rate ratio increases exponentially with decreasing

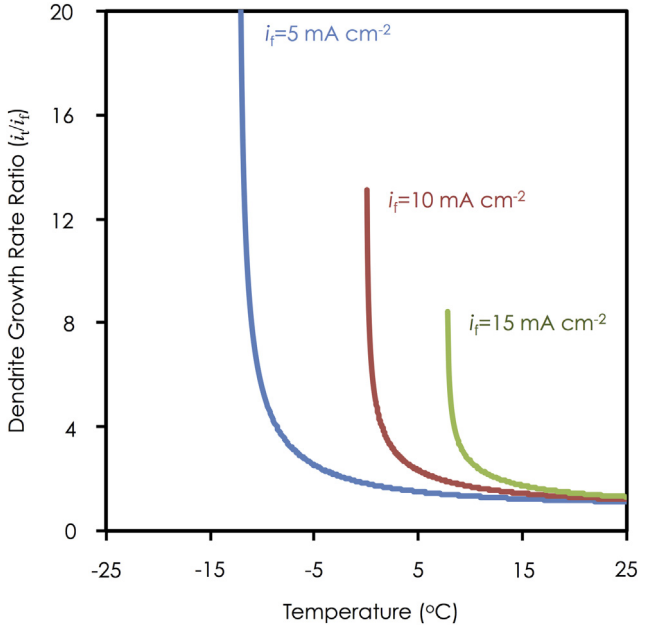


**Fig. 4.** The ratio of the current density at the dendrite tip ($i_t$) to that at the flat electrode surface ($i_f$) plotted as a function of the system temperature. Three curves, representing different Li plating rates of 5, 10 and 15 mA cm$^{-2}$ are shown. It is observed that the critical temperature at which an exponential increase in the dendrite growth rate ratio ($i_t/i_f$) is triggered depends on the Li plating rate. Lower Li plating rates allow a larger temperature window of operation, while higher Li plating rates require operation close to the ambient temperature to prevent uncontrolled dendrite formation.

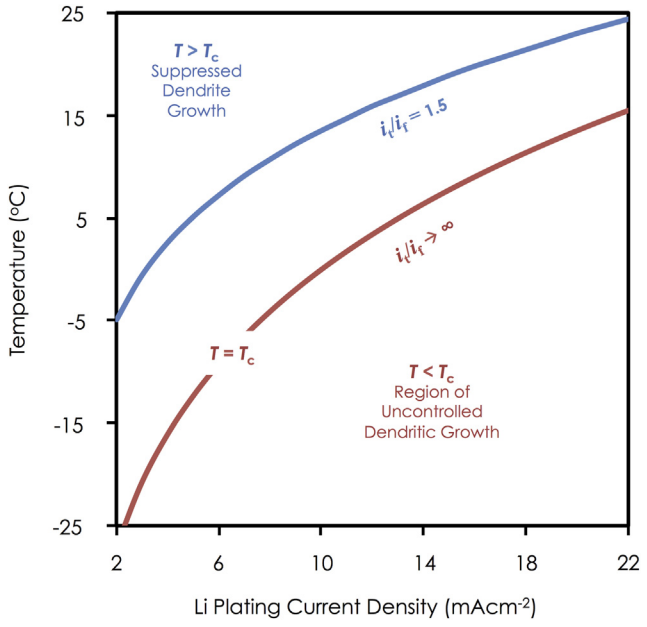


**Fig. 5.** Variation of the dendrite growth rate ratio $i_t/i_f$ with temperature and Li plating current density. The red curve (corresponding to $i_t/i_f \rightarrow \infty$) represents the critical temperature ($T_c$) below which uncontrolled dendritic growth is initiated. The blue curve represents a much lower dendrite growth rate ratio $i_t/i_f = 1.5$. The region above the blue curve can be interpreted as the region of suppressed dendrite growth and stable battery operation (For interpretation of the references to colour in this figure legend, the reader is referred to the web version of this article).

temperature on account of the retarded diffusion (Fig. 2) and the accelerated surface reaction (Fig. 3). As discussed previously, the lower diffusion coefficient (due to higher viscosity and increased ion association) at sub-ambient temperature has the effect of lowering the limiting current density in the system [as per Eq. (6)], thereby exacerbating the lithium-ion depletion at a given plating current density. Furthermore, the reduced SEI thickness at sub-ambient temperature manifests as an increased cathodic transfer coefficient ($\alpha_c$) accelerating the dendrite growth rate [17].

The critical temperature ($T_c$) at which uncontrolled dendritic growth initiates can be defined as the temperature at which the ratio $i_t/i_f \rightarrow \infty$. The current density dependence of the critical temperature is shown in Fig. 5 (red curve representing $i_t/i_f \rightarrow \infty$). The region under the curve represents uncontrolled dendrite growth that is detrimental to lithium battery systems. At a high current density (15 mA cm$^{-2}$), the critical temperature is 8 °C, while at a low current density (5 mA cm$^{-2}$) the critical temperature is about −12 °C. This indicates that Li electrodeposition at a lower current density has a wider temperature window for operation (without dendrite formation) than at a higher current density. Alternatively, lithium battery systems operating at temperatures well below the ambient temperature must be charged at a lower current density (charge rate) to prevent uncontrolled dendrite growth.

## 5. Conclusions

An analytical model for predicting the dendrite growth rate during lithium electrodeposition at sub-ambient temperature is presented. The model extends a prior theoretical framework outlined by the author [17]. A steady-state diffusion–reaction model provides the ratio of the dendrite tip current density to the current density on the flat lithium surface. Since diffusion and surface reaction are temperature-dependent processes (due to temperature

effects on viscosity, ion association and the surface SEI thickness), the dendrite growth rate ratio can be employed to study the temperature-dependence of the dendritic growth process. Following key conclusions can be drawn:

(i) Dendritic growth during lithium plating is accelerated at sub-ambient temperature due to the increased mass transport resistance on the lithium ions, and reduced surface reaction resistance offered by a thinner SEI layer.
(ii) At a given applied current density (corresponding to a battery charging rate), the model predicts a critical temperature below which uncontrolled dendrite formation is initiated. The critical temperature sets the lower bound on the temperature window of operation of a lithium battery.

While no dendrite growth rate data is presently available to compare directly to model predictions, the general trends predicted by the model agree qualitatively with experimental findings [11–13]. Careful measurements of the temperature-dependent diffusion coefficient and charge transfer coefficient along with accurate measurements of the dendrite propagation rates at sub-ambient conditions are being pursued to supplement the findings presented herein.

## References

[1] B. Scrosati, J. Garche, J. Power Sources 195 (2010) 2419–2430.
[2] P. Andrei, J. Zheng, M. Hendrickson, E. Plitchta, J. Electrochem. Soc. 159 (6) (2012) A770–A780.
[3] K. Xu, Chem. Rev. 104 (2004) 4303–4417.
[4] D. Aurbach, E. Zinigrad, Y. Cohen, H. Teller, Solid State Ionics 148 (2002) 405–416.
[5] A. Heller, The Electrochemical Society Interface. Summer, 2013.
[6] O. Crowther, A. West, J. Electrochem. Soc. 155 (11) (2008) A806–A811.
[7] K. Nishikawa, T. Mori, T. Nishida, Y. Fukunaka, M. Rosso, T. Homma, J. Electrochem. Soc. 157 (11) (2010) A1212–A1217.
[8] M. Ishikawa, S. Machino, M. Morita, J. Electroanal. Chem. 473 (1999) 279–284.
[9] T. Nishida, K. Nishikawa, M. Rosso, Y. Fukunaka, Electrochim. Acta 100 (2013) 333–341.
[10] H. Park, C. Hong, W. Yoon, J. Power Sources 178 (2008) 765–768.
[11] H. Ota, K. Shima, M. Ue, J. Yamaki, Electrochim. Acta 49 (2004) 565–572.
[12] H. Ota, X. Wang, E. Yasukawa, J. Electrochem. Soc. 151 (3) (2004) A427–A436.
[13] R. Mogi, M. Inaba, Y. Iriyama, T. Abe, Z. Ogumi, J. Electrochem. Soc. 149 (4) (2002) A385–A390.
[14] C. Brissot, M. Rosso, J. Chazalviel, S. Lascaud, J. Power Sources 81–82 (1999) 925–929.
[15] J. Chazalviel, Phys. Rev. A 42 (1990) 7355.
[16] C. Monroe, J. Newman, J. Electrochem. Soc. 150 (10) (2003) A1377–A1384.
[17] R. Akolkar, J. Power Sources 232 (2013) 23–28.
[18] S. Stewart, J. Newman, J. Electrochem. Soc. 155 (2008) F13–F16.
[19] J. Newman, Electrochemical Systems, Prentice-Hall, Englewood Cliffs, NJ, 1991.
[20] J. Barton, J. Bockris, Proc. R. Soc. (London) A268 (1962) 485–505.
[21] J. Diggle, A. Despic, J. Bockris, J. Electrochem. Soc. 116 (11) (1969) 1503–1514.
[22] L. Ole Valøen, J.N. Reimers, J. Electrochem. Soc. 152 (5) (2005) A882–A891.
[23] M. Ding, K. Xu, S. Zhang, K. Amine, G. Henriksen, T. Jow, J. Electrochem. Soc. 148 (10) (2001) A1196–A1204.
[24] A. Webber, J. Electrochem. Soc. 138 (9) (1991) 2586–2590.
[25] T. Nishida, K. Nishikawa, Y. Fukunaka, ECS Trans. 6 (18) (2008) 1–14.
[26] E. Peled, J. Electrochem. Soc. 126 (1979) 2047.
[27] L. Young, Anodic Oxide Films, Academic Press, New York, 1961.
[28] M. Tang, S. Lu, J. Newman, J. Electrochem. Soc. 159 (11) (2012) A1775–A1785.
[29] H. Ploehn, P. Ramadassand, R. White, J. Electrochem. Soc. 151 (3) (2004) A456–A462.
[30] S. Lee, U. Jung, Y. Kim, M. Kim, D. Ahn, H. Chun, Korean J. Chem. Eng. 19 (4) (2002) 638–644.
[31] M. Ota, S. Izuo, K. Nishikawa, Y. Fukunaka, E. Kusaka, R. Ishii, J.R. Selman, J. Electroanal. Chem. 559 (2003) 175–183.